



HAL
open science

The electrohydrodynamic force distribution in surface AC dielectric barrier discharge actuators: do streamers dictate the ionic wind profiles?

Konstantinos Kourtzanidis, Guillaume Dufour, François Rogier

► To cite this version:

Konstantinos Kourtzanidis, Guillaume Dufour, François Rogier. The electrohydrodynamic force distribution in surface AC dielectric barrier discharge actuators: do streamers dictate the ionic wind profiles?. *Journal of Physics D: Applied Physics*, 2021, 54 (26), pp.26LT01. 10.1088/1361-6463/abf53e . hal-03255410

HAL Id: hal-03255410

<https://hal.science/hal-03255410>

Submitted on 10 Jun 2021

HAL is a multi-disciplinary open access archive for the deposit and dissemination of scientific research documents, whether they are published or not. The documents may come from teaching and research institutions in France or abroad, or from public or private research centers.

L'archive ouverte pluridisciplinaire **HAL**, est destinée au dépôt et à la diffusion de documents scientifiques de niveau recherche, publiés ou non, émanant des établissements d'enseignement et de recherche français ou étrangers, des laboratoires publics ou privés.

ACCEPTED MANUSCRIPT

The ElectroHydroDynamic force distribution in surface AC Dielectric Barrier Discharge actuators: do streamers dictate the ionic wind profiles?

To cite this article before publication: Konstantinos Kourtzanidis *et al* 2021 *J. Phys. D: Appl. Phys.* in press <https://doi.org/10.1088/1361-6463/abf53e>

Manuscript version: Accepted Manuscript

Accepted Manuscript is “the version of the article accepted for publication including all changes made as a result of the peer review process, and which may also include the addition to the article by IOP Publishing of a header, an article ID, a cover sheet and/or an ‘Accepted Manuscript’ watermark, but excluding any other editing, typesetting or other changes made by IOP Publishing and/or its licensors”

This Accepted Manuscript is © 2021 IOP Publishing Ltd.

During the embargo period (the 12 month period from the publication of the Version of Record of this article), the Accepted Manuscript is fully protected by copyright and cannot be reused or reposted elsewhere.

As the Version of Record of this article is going to be / has been published on a subscription basis, this Accepted Manuscript is available for reuse under a CC BY-NC-ND 3.0 licence after the 12 month embargo period.

After the embargo period, everyone is permitted to use copy and redistribute this article for non-commercial purposes only, provided that they adhere to all the terms of the licence <https://creativecommons.org/licenses/by-nc-nd/3.0>

Although reasonable endeavours have been taken to obtain all necessary permissions from third parties to include their copyrighted content within this article, their full citation and copyright line may not be present in this Accepted Manuscript version. Before using any content from this article, please refer to the Version of Record on IOPscience once published for full citation and copyright details, as permissions will likely be required. All third party content is fully copyright protected, unless specifically stated otherwise in the figure caption in the Version of Record.

View the [article online](#) for updates and enhancements.

1
2
3
4
5
6
7
8
9
10
11
12
13
14

The ElectroHydroDynamic force distribution in surface AC Dielectric Barrier Discharge actuators: do streamers dictate the ionic wind profiles?

15 **K Kourtzanidis[‡], G Dufour, F Rogier**

16 ONERA - The French Aerospace Lab, 31000, Toulouse, France

17 E-mail: kourtzanidis@certh.gr
18

19
20 **Abstract.** We show that the spatio-temporal ElectroHydroDynamic (EHD)
21 force production in surface AC-Dielectric Barrier Discharge (AC-DBD) actuators
22 is strongly influenced by both the streamer regime during the positive phase and
23 the micro-discharge regime during the negative phase. Focusing on the spatial
24 EHD force profiles, we demonstrate that the ionic wind spatial distribution can
25 only be explained by the positive contribution of the streamer regime. The
26 location of maximum ionic wind is found to be directly linked with the maximum
27 elongation of the streamers at several millimeters from the exposed electrode. In
28 both positive and negative phases of the AC-DBD operation, residual volumetric
29 and surface charges once again linked to the streamer formation and afterburn,
30 result to a variety of positive EHD force zones which, when time-averaged in one
31 AC period, contribute to the generation of the experimentally observed induced
32 thin wall jet. Through a thorough elaboration of our numerical results, we provide
33 an illustrative explanation of the EHD force spatio-temporal evolution, showcase
34 the importance of streamers and retrieve a correct representation of the ionic wind
35 spatial profiles when compared to experiments.

36 Submitted to: *J. Phys. D: Appl. Phys.*
37
38
39
40
41
42
43
44
45
46
47
48
49
50
51

52 [‡] Present address: CERTH - Centre for Research and Technology Hellas, 57001 Thessaloniki,
53 Greece
54
55
56
57
58
59
60

1. Introduction

ElectroHydroDynamic (EHD) flows induced by surface Alternative Current Dielectric Barrier Discharge (AC-DBD) actuators have found use in a variety of applications mainly as means of aerodynamic flow control [33]. Separation delay and flow re-attachment, turbulent enhancement and laminar-to-turbulent transition control, vortex generation, turbine blades aerodynamic enhancement are a few of such applications. Despite the numerous studies, the spatio-temporal distribution of the induced EHD flow or ionic wind is yet to be fully understood. Experiments have demonstrated that the plasma discharge nature is very different in both half-phases [4]. In the positive going cycle, high current streamer discharges form above the dielectric layer while in the negative going cycle, lower current but higher frequency micro-discharges are present. The contribution of each phase to the EHD force production is a controversial subject. Concerning temporal aspects, push-push [2, 16, 29, 20] and push-pull [10, 27, 41, 39] scenarios have been proposed and supported by experiments and simulations. Push-push theory suggests that both cycles contribute to a positively directed EHD force (x-axis) while push-pull suggests a negative EHD force during the positive going cycle. Although most of these studies agree that the ionic wind velocity is higher in the negative-going cycle, these results alone do not offer much information on the EHD forcing and adequate links (if any) with the discharge behavior. Concerning spatial aspects, on one hand experimental studies have been used to retrieve the force distribution [2, 21, 15, 25, 26]. These studies are mostly based on strong assumptions (pressure gradients, local acceleration, turbulent fluctuations) and an inverse Navier-Stokes (NS) procedure that render the results ambiguous as they do not correlate with velocity measurements. On the other hand, numerical and theoretical studies on the ionic wind profiles show in general good agreement with experiments in terms of overall thrust production but fail to capture the maxima position of the induced wall-jet. Most of these numerical studies suffer from low accuracy due to the numerical schemes used and simplifying assumptions [46] made and/or insufficient spatial discretization while limited information on the spatial distribution of the EHD force has been provided (e.g. Ref. [7], see also references in Ref. [24]). Simplified (and computationally inexpensive) models such as the widely used Suzen-Huang model [48, 47] fail to capture and most importantly explain physically the elongation of velocity maxima. The EHD spatiotemporal distribution along with the location of velocity maxima are important aspects to what concerns flow control applications such the ones described in Ref. [17, 43, 9, 6] including stabilization/cancelation of the shear layer's unstable waves (e.g. Tollmien-Schlichting waves), laminar-to-turbulent transition, separation control, noise reduction etc. where the localization of the SDBD and consequently its induced flow can be a critical design parameter for an optimized control authority. It is worth mentioning that SDBDs can operate in a continuous or burst mode and the latter has been shown [3] to provide both single and double frequency flow fluctuations once again interesting for canceling non-linear waves in turbulent boundary layers and wakes.

In this work, based on the detailed numerical simulations of our recently published work in Ref. [24], we answer two important questions on the spatio-temporal uncertainty of EHD force and ionic wind produced by surface AC-DBD discharges : Why the ionic wind spatial profiles present maxima at a distance of several millimeters from the exposed electrode as observed experimentally [53, 10, 14, 20]? How does each phase of the AC cycle contribute to the EHD production zones (magnitude

and direction) and what are the implications on the ionic wind spatial profiles? We note again that numerous studies have dealt with the characterization of the SDBD thrust generation as well as the unsteady flow and forcing inside an AC period. In addition, the authors in Ref. [11], investigated the influence of streamers inhibition to the induced flow, demonstrating that when streamers are not present (as in the case of a thin wire-to-plane SDBD) the velocity increases in both cycles and the maximum velocity is produced in the positive going cycle. The total produced thrust also increases in the case of streamer inhibition. Here we do not aim to characterize the influence of streamers on the EHD force magnitude compared to a case without streamers but to investigate their influence on EHD production in the typical case of AC-SDBD discharges with plate-to-plate electrodes (the majority of SDBD actuator studies only focus on such configurations). To do so, we build and elaborate on the results of our recently published work in Ref. [24], demonstrate the time-averaged spatial EHD force and ionic wind produced by an AC-DBD actuator and propose an illustrative explanation of the complex plasma-flow interaction.

2. Methods

A self-consistent modeling approach has been followed in order to obtain the full cycle characteristics of the surface AC-DBD operation. Details on the numerical and physical models used as well as discussion on the main assumptions made can be found in Ref. [13, 24]. Briefly, the computational solver used in this paper is COPAIER, a multi-species and multi-temperature plasma fluid solver allowing for self-consistent description of the plasma spatial and temporal evolution. The continuity equation in a drift-diffusion formulation is solved for each species modeled (here electrons, positive and negative ions) coupled with Poisson's equation and an electron energy equation under the local mean energy approximation. The reactions considered include ionization, 2-body attachment, 3-body attachment, e-ion recombination, ion-ion recombination. Appropriate boundary conditions are implemented to ensure the self-consistency of the simulation (including secondary electron emission and dielectric charging). Similar physical models have been used extensively in the simulation of AC-SDBDs in atmospheric air (Ref. [7, 37, 38, 1, 36]) providing sufficient agreement with experimental findings for the purpose of this work. We note that two of the major assumptions made in the current modeling the SDBD are the neglect of photoionization and the assumption of two-dimensional evolution. Both of these assumptions have been discussed thoroughly in Ref. [24]. On one hand, photoionization's influence on streamer initiation and propagation (as well as sustainability of corona regime) is expected to be significant, but its effects are expected to be limited to faster initiation of the discharge and longer elongation of the streamer [28]. Ref. [30] also confirms the reduced influence of the photoionization in the overall physics of surface DBD actuators. Considering the focus of this paper on physical insights and not an one-to-one comparison with experiments along with the ambiguity of photoionization models under high electric fields, we leave a more detailed study including photoionization for a future work. On the other hand, the nature of the surface DBD is three-dimensional (3D). Discharges (both streamers and microdischarges) are initiated on spots of the exposed electrode with intervals on the third-dimension which are linked to chaotic procedures and impurities of the electrodes. Three-dimensional simulations in Ref. [40] using artificial disturbances to initiate the spanwise non-uniform discharges have revealed that the average spatiotemporal evolution of the body force (which strongly

relates to charge and electric field distribution) is well reproduced by the 2D models despite the non-uniformity observed. Moreover, experiments have demonstrated that neighboring discharges in the spanwise dimension are typically located several mm (see Ref. [4] for example) apart possibly underlying a self-organizing structure of the spanwise discharge which eliminates high interference. Therefore, the 2D approximation used in this study can be considered as a relatively good approximation for the evolution of both the streamer and the microdischarge regimes but 3D simulations are essential to reveal the complex flow structure induced by the SDBD actuator.

The AC-DBD under study is a 100 kHz, 15 kV actuator. The operating frequency is higher than the ones typically used in experiments (1-25 kHz) allowing for reducing the computational burden of our simulations (typical CPU times for 4 periods of operation range between 1 and 2 months over 100 CPU cores). The reader should refer to Ref. [24] for a discussion on the AC frequency influence on our results.

We note that the goal of this work is not to parametrize the SDBD operation and induced flow on important aspects such as the applied frequency and voltage amplitude. Such studies require a series of simulation runs which (taking into account the huge CPU cost of a single simulation) render this task extremely time-consuming. Development of reduced order models (based on data driven/AI/Machine Learning techniques such as neural networks etc [32, 42]) allowing for fast and accurate results is out of the scope of this work. In addition to the fact that these algorithms need to be fed by detailed simulations such the one described in Ref. [24], the latter can provide insights on the EHD force production as the results of this current work demonstrate. For information on the plasma characteristics and EHD force parametrization over various operational parameters, the reader is referred to the literature on both experimental and numerical (with simplified models) studies (Ref. [4, 18, 45]).

3. Time-dependent plasma characteristics and EHD force production zones during an AC cycle

In Ref. [24], we show that the AC-DBD operation can be decomposed in two phases which are nevertheless strongly inter-connected in agreement with several experimental studies [33, 4]. In summary our findings demonstrate that: In the positive phase, a positive corona-like discharge forms at the active electrode interrupted by a high current surface streamer discharge. The streamer propagates detached from the dielectric surface acting as a virtual anode. When its propagation is stopped, it slowly relaxes and positive ions from its body charge the dielectric surface contributing to an elongated zone of positive potential and consequent high electric field at a distance of several millimeters from the active electrode. In the negative phase, volumetric charge separation leads to the initiation of repetitive microdischarges which attach to the active electrode (cathode in this phase) forming a thin cathode layer. Each microdischarge terminates with the propagation of a thin plasma layer attached to the dielectric surface. The positively charged portion of the dielectric which persists from the positive/streamer phase, pulls this layer further and further until it is quenched due to electrons and negative ions which drift towards the dielectric. In the relaxation phase between consecutive microdischarges, positive ions are repelled outwards from the dielectric surface and the thin ion layer attached to the dielectric consists of mainly negative ions.

Based on the aforementioned discharge characteristics, we can identify the EHD force production zones during the two-phase operation of the AC-DBD actuator. In Fig. 1 and Fig. 2 we present schematically the EHD force production zones in the positive and negative phase respectively. We note that dimensions are not in scale and the representation is illustrative: not all ion cloud zones are presented but only the most important for the EHD force production. The instantaneous EHD force vectors presented in Fig. 4, 9 and 15 of Ref. [24] along with the detailed operational description therein help us construct the discussion presented below. The instantaneous EHD force per unit volume is given by [8]:

$$\vec{F}_{EHD} = q(n_+ - n_- - n_e)\vec{E} \quad (1)$$

where q is the elementary charge, n_+ , n_- and n_e are the positive, negative ions and electrons density respectively and \vec{E} is the electric field vector. It is clear that the EHD force is generated in regions with high electric fields, without charge neutrality and high unipolar charge concentration.

In the following discussion, F_{x+} and F_{x-} refer to the positive and negative parts of the EHD force's x-component, while F_{y+} and F_{y-} to the positive and negative parts of the EHD force's y-component respectively. During the positive phase, the EHD force is located inside 3 main regions: First, the positive ion cloud expanding over the dielectric. Second, the streamer head and the streamer sheath region between its body and the dielectric surface during its short-term propagation. Third, an important part of the EHD force is located in the zone ahead of the streamer maximum elongation length during the relaxation phase. The latter is due to the conductive nature of the streamer and the positive dielectric charging during the (long-term) relaxation phase of the streamer discharge. Both of these factors lead to a zone of enhanced electric field just downstream the streamer body, promoting ionization, positive-ion production which along with the diffusion of the latter from the streamer body contribute to a positive x-directed EHD forcing (F_{x+}), as the positive voltage phase persists. The x-directed component is positive in all three regions while a negative region of y-directed force (F_{y-}) exists in the sheath region between the streamer body and the dielectric. Phase C as illustrated in Fig. 1 contributes the most to the EHD force as it lasts several 100s of ns.

During the negative phase, the EHD force is located inside two main regions: First, the negative ion cloud as a remnant of the positive phase streamer with an important x-directed positive component (F_{x+}) inside a region near the dielectric and between the charged dielectric portions. Second, inside the cathode sheath layer formed due to each micro-discharge generation. The force there is strongly negative and mainly x-directed (F_{x-}) as positive ions dominate. In addition, during the relaxation phase between each microdischarge inside the thin negative ion layer attached to the dielectric. This layer expands further and further after each microdischarge pulse as the electric field between the surface charged regions progresses along. A positive x-directed force (F_{x+}) and a negative y-directed force (F_{y-}) dominate in this region. By the end of the negative phase, the region once covered by the streamer discharge is now covered by ion clouds and the thin negative layer near the dielectric which is now negatively charged all along. In all phases, dielectric charging plays an important role in both the discharge behavior as well as the electric field enhancement in critical regions for EHD force production. The reader may find additional details in the captions of Fig. 1 and Fig. 2.

In the following section, the spatiotemporal distribution of the EHD force is

6

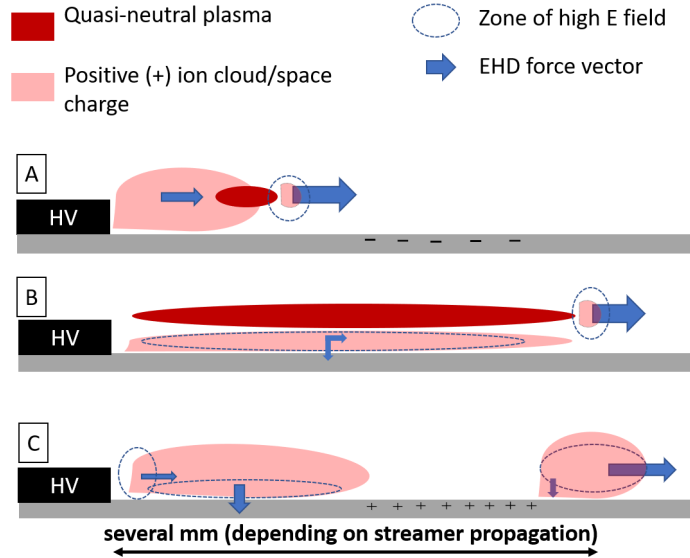


Figure 1. Illustration of the positive phase EHD force production zones: A) Initially the positive ion cloud expands over the dielectric surface until space charge effects initiate the quasi-neutral streamer. A positive space charge and high electric field region exists at the head of the streamer. B) The streamer propagates quickly parallel to the dielectric surface. In addition to the space charge at its head, a zone of high electric field populated by diffused positive ions exist as a sheath between the streamer body and the dielectric. C) At the relaxation phase, the streamer relaxes and charges the dielectric positively. The virtual anode formation due to the streamer (after-burn) and dielectric charging (relaxation) enhances the electric field at a distance of several millimeters and leads to an elongated zone of EHD force production. The analysis is based on our detailed simulations of Ref. [24].

presented and analyzed, in order to validate the analysis presented above along with the ionic wind spatial profiles obtained through CFD simulations.

4. Results and discussion

4.1. EHD force distribution - Temporal aspects

The space-integrated EHD force (x and y component) versus time (during the third period of actuation) extracted from the detailed simulations of Ref [24], is shown in Fig. 4. The effects of both the streamer and micro-discharges are quite remarkable : The x-directed force is strongly negative (F_{x-}) during each micro-discharge formation while it becomes positive (F_{x+}) in the relaxation phase (thin layer propagation) during the negative going cycle. In the positive going cycle the x-force is always positive (F_{x+}) and the streamer produces a pulse of positive force. The streamer discharge seems to have a very important influence on the y-force : While the y-force remains a lot weaker than the x-component, each streamer produces a significant negative y-force (F_{y-}) which seems to be in good agreement with the unsteady y-directed velocity measurements in Ref. [4].

This suggests that the definition of the EHD forcing as a push-push or push-

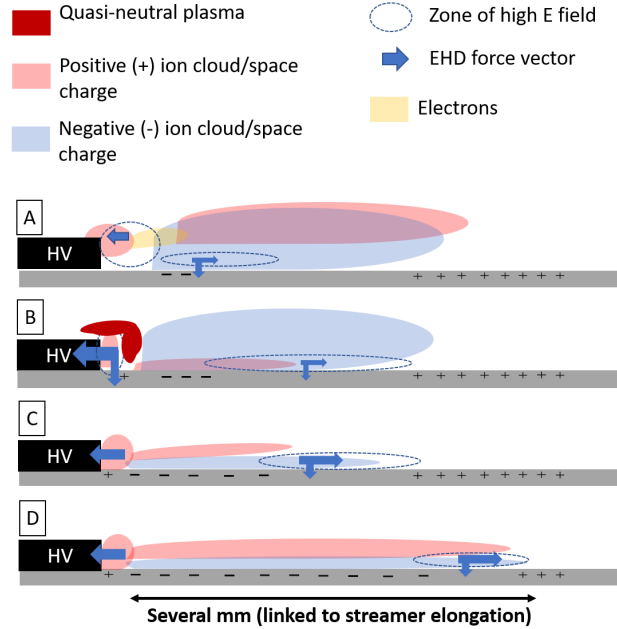


Figure 2. Illustration of the negative phase EHD force production zones: A) Electrons produced near the active electrode drift towards the dielectric charging it negatively. Positive ions near the cathode contribute to a negative mainly x-directed EHD force (F_{x-}). The negative ion cloud region near the dielectric (remnant from the positive phase) produces positive x-directed EHD force (F_{x+}) under the influence of the electric field due to the potential difference between the negative and positive charged portions of the dielectric surface. B) A quasi-neutral micro-discharge forms and rapidly attaches to the exposed electrode forming a cathode layer. The cathode layer holds very high electric fields, positively dominated space charge and a negative EHD forcing (F_{x-} , F_{y-}) zone appears. Positive ions are generated in the near surface region due to the previously mentioned electric field. C) Once the micro-discharge relaxes and the plasma layer propagates on the dielectric surface, positive ions are repelled from the dielectric leaving a negative ion layer behind. The EHD force is there positive in the x-direction (F_{x+}) and negative in the y-direction (F_{y-}) and dominant due to the time-scale of the relaxation phase between each microdischarge. D) The surface ion layer expands after each microdischarge until it reaches the end of the positively charged portion of the dielectric (linked to the streamer elongation during the positive phase). The analysis is based on our detailed simulations of Ref. [24].

pull action is misleading. Both phases contribute positively to the EHD x-directed force (F_{x+}) but strong negative parts exist during the negative phase too. As we will see below at the spatial distribution and resulting ionic wind profiles, the negative parts can form zones of strong negative flow (at least under the operational conditions studied here). Moreover, the y-directed forcing is negative (F_{y-}) throughout the AC cycle. We consider safe to speculate that depending on various operational characteristics (applied voltage, AC frequency, dielectric material, electrode thickness), the AC-DBD might favor the positive or negative parts during the negative phase resulting to push-push or push-pull effects. Thus, the temporal forcing or velocity profiles extracted from experiments should take into account these

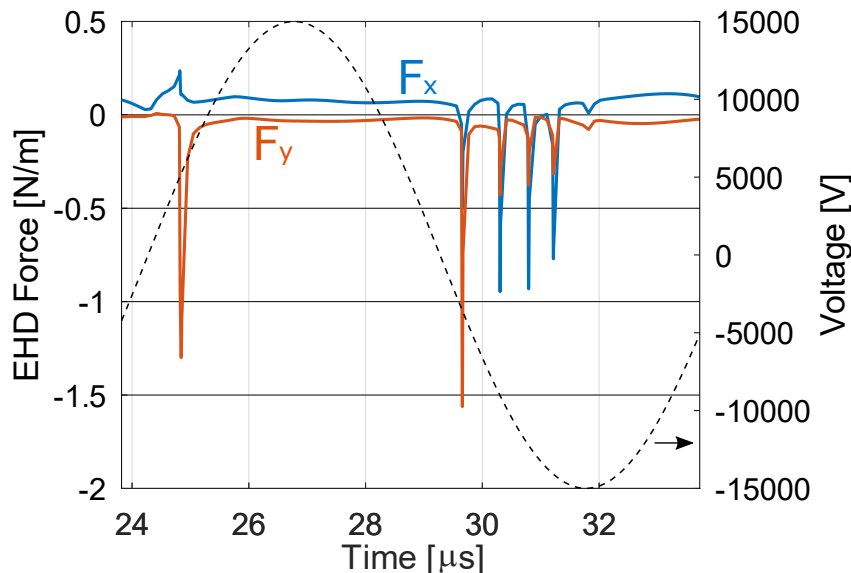


Figure 3. Space integrated EHD force (x and y components) [N/m] vs Time [μs] inside a full AC cycle (3rd period- see Ref. [24]). The voltage waveform is also depicted with the black dashed line.

operational parameters and relevant time-scales as well as the measurement locations for both velocity components.

4.2. EHD force distribution - Spatial aspects

As the fluid response takes place in much longer time-scales than these two phases and the AC frequency of operation, the time-averaged EHD-force provides a good representation of the continuous EHD forcing and resulting flow. The time-averaged force has been calculated during an AC period (third period of Ref. [24]) and its spatial distribution (magnitude, x and y components) are plotted in Fig. 4 and Fig. 5. Note that the force components have been plotted separately for positive and negative values for visualization purposes (see captions of Fig. 4 and Fig. 5 for more details). The EHD force occupies a volume of approx. 4-5 mm in x-direction (F_x) and 1.5-2 mm in y-direction (F_y). It is very high in a small volume near the exposed electrode where it is mainly negative-directed (both in x (F_{x-}) and y (F_{y-}) directions). The X-directed EHD force is positive (F_{x+}) and important inside three regions. The first is linked to the initiation of the streamer discharge - the zone at a distance of approx. 0.5 mm where strong ionization occurs. The second is a zone very close to the dielectric layer where negative ions exist during the negative phase. The third is the zone in front of the streamer final elongation length linked to its propagation and dielectric charging during the positive phase. It is thus obvious that the positive going cycle (streamer regime) has important implications to the EHD force production and especially to its spatial distribution in both phases. The negative x-directed EHD force (F_{x-}) zone

near the exposed electrode is linked to the cathode layer formation during the negative phase. This zone is also very important and simplified models often neglect it. The negative y-directed EHD force (F_{y-}) is located mainly close to the active electrode and a layer attached to the dielectric. This zone is due to both phases (positive charges accelerated into the streamer sheath during the positive phase and negative ion charging drifting towards the dielectric as the thin layer moves downstream during the negative phase). The reader should refer to Ref. [24]) for more details on the discharge evolution in each AC subcycle which support all of the above. The total length of the EHD force reaches approx. 4mm while the EHD force zone linked to the enhanced electric field ahead of the streamer discharge occupies a zone of approx. 0.8 mm. We note that the streamer discharge maximum elongation is approx. 3.5 mm. To our knowledge this is the first time that such a result has been obtained - one that links the EHD force distribution with the streamer regime and demonstrates the experimentally observed elongation of the EHD forcing (see Ref. [5] for example). We also note that a longer streamer elongation (due to photoionization effects or streamer pulse repetition during the positive phase under lower actuation frequency) should reproduce similar effects and elongate the EHD force localization even more. As streamers have been experimentally observed to propagate at distances in the order of 10 mm, we speculate that our results should translate to such cases owing to the physical principles of our proposed EHD forcing scheme.

4.3. Ionic wind spatial profiles

The time-averaged EHD body force term has been incorporated into a CFD solver (openFOAM [49]) in order to calculate the flow field resulting from the AC-DBD actuators (Fig. 6). We note here that the total time-averaged space-integrated x-directed force (F_x) is 64 mN/m while the total y-directed force (F_y) is -45 mN/m. Menter's $k-\omega$ Shear Stress Transport (SST) turbulence model [31] is used for solving the Reynolds-averaged Navier-Stokes equations (RANS) which has already been proven adequate for surface AC-DBD induced wall-jet flows [23, 22] (unsteady calculations are out of scope for this work although essential for a direct comparison with experimental measurements). Fig. 6 presents the steady-state velocity contours while Fig. 7 the corresponding velocity profiles at a distance of 3 mm, 1, 2 and 3 cm from the exposed electrode edge. The wall jet flow reaches maximum speeds at a height of approx. 0.5 mm (for 2 and 3 cm) from the dielectric surface in good agreement to experimentally obtained velocity profiles (see Ref. [33] and references therein). The thickness of the boundary layer wall jet ranges from 1-2 mm. The maximum velocity occurs at a distance of approx. 4.5 mm from the exposed electrode as can be seen from the zoomed sub-figures in Fig. 6. To our knowledge, this result is also novel: Not only it clearly demonstrates the importance of the streamer propagation and subsequent dielectric charging (in both phases as described in Ref. [24]) to the ionic wind spatial profile but it also explains the experimental profiles in a physical manner linked to the plasma formation and not purely to fluid dynamics. The maximum length of the EHD force (approx. 4 mm) and the resulting (positive) ionic wind maximum at a distance of 4.5 mm are linked with the enhanced electric field zone just ahead of the maximum elongation length of the streamer discharge, showcasing its influence on the ionic wind spatial distribution. We note here that Ref. [34], Ref. [12] and Ref. [44] point out towards this direction too. We also note that the maximum elongation distance of the streamer discharge is subject to various parameters (AC frequency, applied

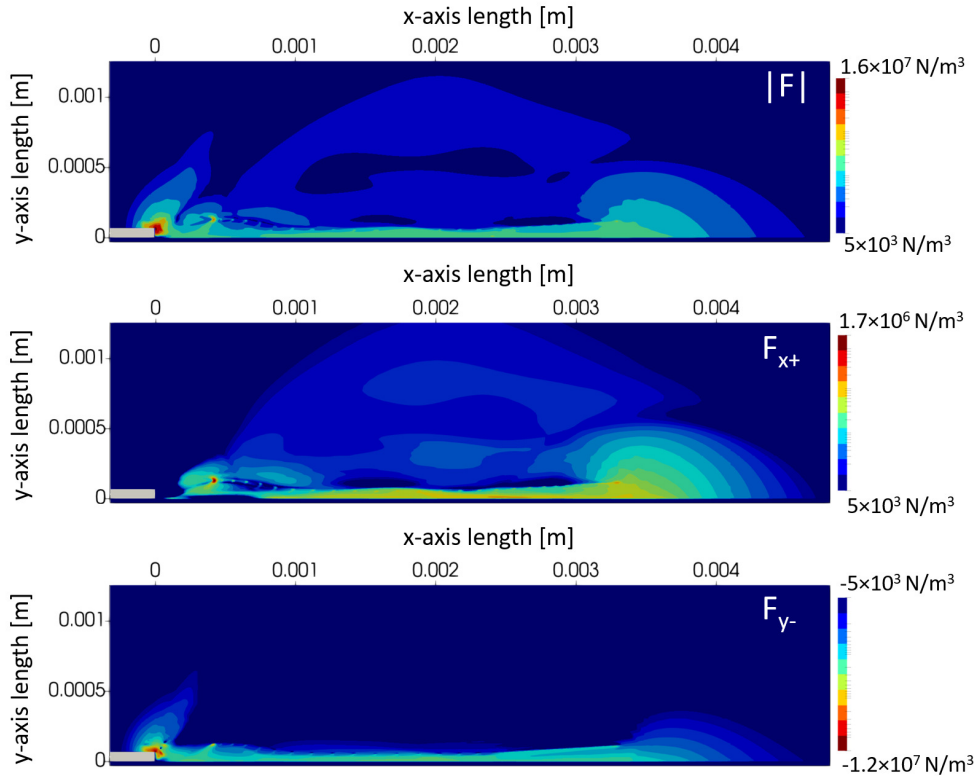


Figure 4. Time-integrated (over 1 AC period) EHD force distribution - Force magnitude and F_{x+} (x-component, positive part), F_{y-} (y-component, negative part) components [N/m^3 , log-scale - scaled to min of $1000 \text{ N}/\text{m}^3$ (or max of $-1000 \text{ N}/\text{m}^3$ for the negative parts) for visualization purposes]. Note that for F_{y-} , we have used the expression $\text{sgn}(F_y)\lg(\text{abs}(F_y))$ in order to represent the spatial distribution in a log scale. The maximum length of the EHD force zone ($\approx 4 \text{ mm}$) coincides with the enhanced electric field zone ahead of the streamer's maximum elongation length during the positive phase.

voltage, dielectric constant and thickness) and thus the maximum of the ionic wind can be found quite further downstream for different test cases. This result is in good agreement with the experimental profiles retrieved in various studies [53, 19, 10, 14, 20] which indicated that the maximum velocity occurs at a distance of several millimeters downstream the exposed electrode and could not be replicated so far by similar numerical experiments such as in Ref. [7]. We emphasize again that the AC frequency studied here is high compared to most of the aforementioned studies but this fact should have only quantitative effects on the EHD force. A lower frequency (under same applied voltage) leads to several streamers and more microdischarges in both subcycles. Qualitatively, and focusing on the positive phase, each streamer will go through a preburn (glow/corona like regime), burn and afterburn (relaxation) phase. Therefore, we consider safe to speculate that the effect of streamers on the EHD force distribution in lower operating frequencies should be even more pronounced. Nevertheless, simulations at lower frequencies are necessary to confirm and validate this claim. . In addition, a negative flow region is observed initiated near the exposed

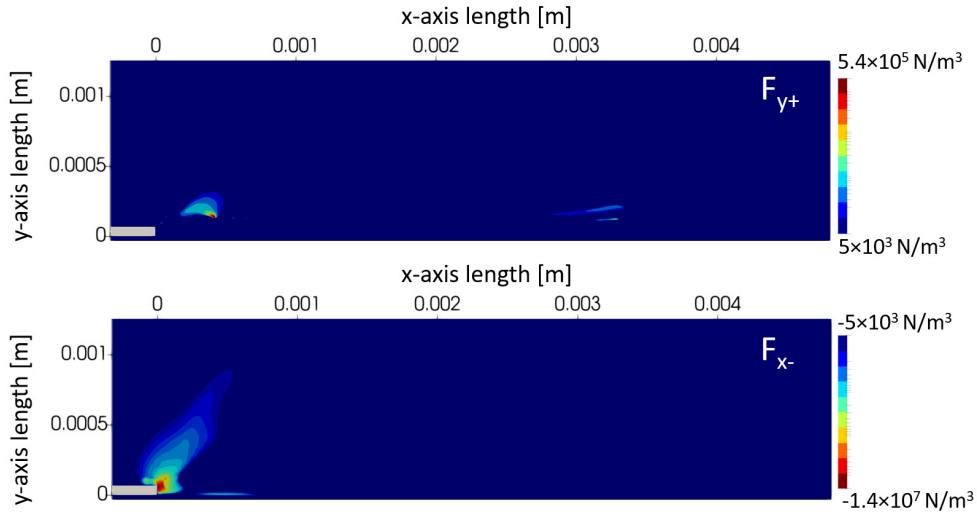


Figure 5. Time-integrated (over 1 AC period) EHD force distribution - F_{y+} (y-component - positive part), F_{x-} (x-component - negative part) components [N/m^3 , log-scale - scaled to min of $1000 \text{ N}/\text{m}^3$ (or max of $-1000 \text{ N}/\text{m}^3$ for the negative parts) for visualization purposes]. Note that for F_{x-} , we have used the expression $\text{sgn}(F_x)\text{lg}(\text{abs}(F_x))$ in order to represent the spatial distribution in a log scale. The strong negative x-force near the exposed electrode is apparent.

electrode - limited in volume compared to the positive flow. This thin jet flow, induced by the strongly negative EHD zone near the electrode as we have seen, might indicate that opposing flows are present in DBD actuators - another aspect that needs further investigation and might have been ignored so far, an aspect that surely depends on dimensioning (e.g. electrode thickness) and location of measurements/control volume choice. We note finally that the high velocities obtained compared to the experimental results (as well as the thinner jet profiles) are directly linked to the high AC frequency used in the simulations - the goal of this study is the qualitative explanation of the spatial profiles and discrepancies observed which can be extrapolated to lower frequencies without loss of generality. We have already validated this by scaling the EHD force magnitude and manage to reproduce velocity magnitudes and profiles that agree with experimental values. In any case, the reader is referred to Ref. [24] for a detailed analysis of each phase along with charge evolution, electric field and surface charging distributions at different time instants as well as discussion on assumptions made.

Our results indicate that streamers if properly controlled can be used to create localized flow disturbances and explain why if coupled with adequate DC fields they can possibly enhance the EHD force (Ref. [44]), even though in a typical AC-SDBD operation positive streamers have been linked to reduced magnitude of ionic wind. Thus, improved actuators can be designed based on repetitive streamer production and subsequent charge drift. The influence of streamers to EHD force production is under study in simplified configurations such as point-to-plane discharges. Recently it has been demonstrated experimentally [35] that in such configurations, streamers have a strong positive effect on the EHD force magnitude and consequent ionic wind - in contrast to SDBDs. The reasons behind this difference in these configurations has not

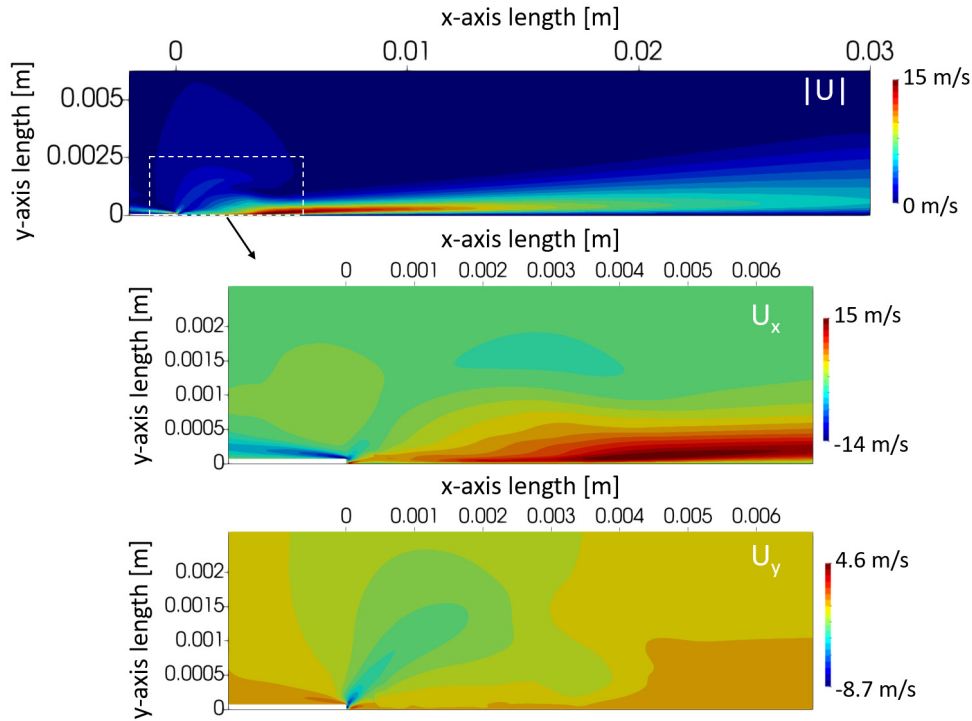


Figure 6. Steady state flow field - Velocity magnitude contours [m/s] and zoom near the HV electrode zone. The formation of the wall jet and position of maximum positive velocity are directly linked with the maximum elongation length of the streamer discharge and the enhanced field downstream during the positive phase.

been revealed yet and thus additional effort (both experimental and numerical) should be put towards this aspect. Revealing the complex physics behind EHD production in atmospheric pressure corona and streamer discharges (with or without dielectric barrier) can lead to optimized devices finding application in in-atmosphere propulsion systems replacing typical corona based ionic propulsion systems [52, 50, 51].

5. Conclusion

We provided an explanation for the ionic wind spatial profiles induced by surface AC-DBD actuators. Based on our previously reported detailed numerical study of the surface AC-DBD actuator, we demonstrated that the elongation of the EHD force and local maxima of the ionic wind are mainly due to the streamer regime of the positive phase but also the presence of a thin negative ion layer during the negative phase attached to the dielectric (which also links to the streamer regime). Dielectric charging plays a crucial role on the volumetric charge redistribution and consequent EHD force production zones. A strong negative force region also exists near the exposed electrode linked mostly to the negative phase (micro-discharge formation). Therefore, a push-push or pull-pull scenario should depend on the localization of the measurements as well as the operational characteristics of the actuator. We have

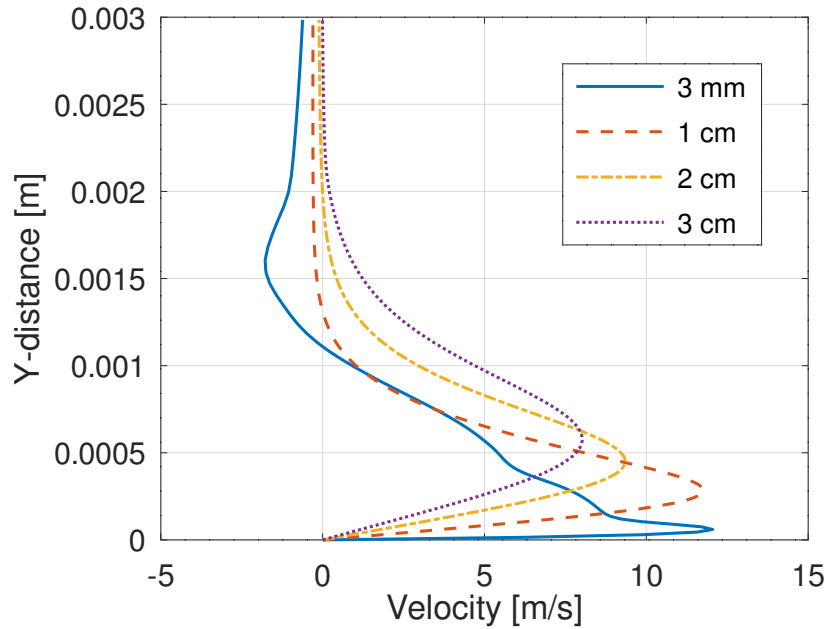


Figure 7. Velocity profiles at 3 mm, 1 cm, 2 cm and 3 cm from the HV electrode

proposed a detailed explanation behind the EHD production zones and backed up our claims with numerically extracted profiles of the EHD force and the ionic wind. Apart of the obvious implications to aerodynamic flow control, several domains can leverage such findings to control and improve EHD flows, create novel devices and even replace typical corona based EHD thrusters for in-atmosphere propulsion systems.

Acknowledgments

This work has received funding under the E.U. MSCA-RISE - Marie Skłodowska-Curie Research and Innovation Staff Exchange (RISE) scheme as part of the project ‘Control of Turbulent Friction Force’ (CTFF) - Grant agreement ID: 777717.

References

- [1] M. Abdollahzadeh, J. Pascoa, and P. Oliveira. Implementation of the classical plasma–fluid model for simulation of dielectric barrier discharge (dbd) actuators in openfoam. *Computers & Fluids*, 128:77–90, 2016.
- [2] N. Benard, A. Debien, and E. Moreau. Time-dependent volume force produced by a non-thermal plasma actuator from experimental velocity field. *Journal of Physics D: Applied Physics*, 46(24):245201, 2013.
- [3] N. Benard and E. Moreau. Capabilities of the dielectric barrier discharge plasma actuator for multi-frequency excitations. *Journal of Physics D: Applied Physics*, 43(14):145201, 2010.
- [4] N. Benard and E. Moreau. Electrical and mechanical characteristics of surface ac dielectric barrier discharge plasma actuators applied to airflow control. *Experiments in Fluids*, 55(11):1846, 2014.
- [5] N. Benard, P. Note, M. Caron, and E. Moreau. Highly time-resolved investigation of the electric

- wind caused by surface dbd at various ac frequencies. *Journal of Electrostatics*, 88:41–48, 2017.
- [6] N. Benard, J. Pons-Prats, J. Periaux, G. Bugada, P. Braud, J. Bonnet, and E. Moreau. Turbulent separated shear flow control by surface plasma actuator: Experimental optimization by genetic algorithm approach. *Experiments in Fluids*, 57(2):22, 2016.
- [7] J. Boeuf, Y. Lagmich, T. Unfer, T. Callegari, and L. Pitchford. Electrohydrodynamic force in dielectric barrier discharge plasma actuators. *Journal of Physics D: Applied Physics*, 40(3):652, 2007.
- [8] J. Boeuf and L. Pitchford. Electrohydrodynamic force and aerodynamic flow acceleration in surface dielectric barrier discharge. *Journal of Applied Physics*, 97(10):103307, 2005.
- [9] T. C. Corke, C. L. Enloe, and S. P. Wilkinson. Dielectric barrier discharge plasma actuators for flow control. *Annual review of fluid mechanics*, 42:505–529, 2010.
- [10] A. Debien, N. Benard, L. David, and E. Moreau. Unsteady aspect of the electrohydrodynamic force produced by surface dielectric barrier discharge actuators. *Applied Physics Letters*, 100(1):013901, 2012.
- [11] A. Debien, N. Benard, and E. Moreau. Streamer inhibition for improving force and electric wind produced by dbd actuators. *Journal of Physics D: Applied Physics*, 45(21):215201, 2012.
- [12] E. Defoort, R. Bellanger, C. Batiot-Dupeyrat, and E. Moreau. Ionic wind produced by a dc needle-to-plate corona discharge with a gap of 15 mm. *Journal of Physics D: Applied Physics*, 53(17):175202, 2020.
- [13] G. Dufour and F. Rogier. Numerical modeling of dielectric barrier discharge based plasma actuators for flow control: the copaier/cedre example. *AerospaceLab*, 2015.
- [14] R. Durscher and S. Roy. Evaluation of thrust measurement techniques for dielectric barrier discharge actuators. *Experiments in fluids*, 53(4):1165–1176, 2012.
- [15] C. Enloe, M. McHarg, and T. E. McLaughlin. Time-correlated force production measurements of the dielectric barrier discharge plasma aerodynamic actuator. *Journal of applied physics*, 103(7):073302, 2008.
- [16] M. Forte, J. Jolibois, J. Pons, E. Moreau, G. Touchard, and M. Cazalens. Optimization of a dielectric barrier discharge actuator by stationary and non-stationary measurements of the induced flow velocity: application to airflow control. *Experiments in Fluids*, 43(6):917–928, 2007.
- [17] K. Fujii. Three flow features behind the flow control authority of dbd plasma actuator: Result of high-fidelity simulations and the related experiments. *Applied Sciences*, 8(4):546, 2018.
- [18] S. Grosse and D. Angland. Parametric investigation of the fluid mechanic performance of an ac dielectric barrier discharge plasma actuator. *Journal of Physics D: Applied Physics*, 53(45):455202, 2020.
- [19] J. Jolibois and E. Moreau. Enhancement of the electromechanical performances of a single dielectric barrier discharge actuator. *IEEE Transactions on Dielectrics and Electrical Insulation*, 16(3):758–767, 2009.
- [20] M. Kotsonis and S. Ghaemi. Performance improvement of plasma actuators using asymmetric high voltage waveforms. *Journal of Physics D: Applied Physics*, 45(4):045204, 2012.
- [21] M. Kotsonis, S. Ghaemi, L. Veldhuis, and F. Scarano. Measurement of the body force field of plasma actuators. *Journal of Physics D: Applied Physics*, 44(4):045204, 2011.
- [22] K. Kourtzanidis. Numerical simulation of plasma actuators for flow control. In *51st AIAA Aerospace Sciences Meeting including the New Horizons Forum and Aerospace Exposition*, page 134, 2013.
- [23] K. Kourtzanidis. *Modélisation numérique d’actionneurs plasma pour le contrôle d’écoulement*. PhD thesis, 2014.
- [24] K. Kourtzanidis, G. Dufour, and F. Rogier. Self-consistent modeling of a surface ac dielectric barrier discharge actuator: In-depth analysis of positive and negative phases. *Journal of Physics D: Applied Physics*, 54(4):045203, 2020.
- [25] J. Kriegseis, C. Schwarz, A. Duchmann, S. Grundmann, and C. Tropea. Piv-based estimation of dbd plasma-actuator force terms. In *50th AIAA aerospace sciences meeting including the new horizons forum and aerospace exposition*, page 411, 2012.
- [26] J. Kriegseis, C. Schwarz, C. Tropea, and S. Grundmann. Velocity-information-based force-term estimation of dielectric-barrier discharge plasma actuators. *Journal of Physics D: Applied Physics*, 46(5):055202, 2013.
- [27] M. Kuhnhehn, B. Simon, I. Maden, and J. Kriegseis. Interrelation of phase-averaged volume force and capacitance of dielectric barrier discharge plasma actuators. *Journal of Fluid Mechanics*, 809, 2016.
- [28] A. Likhanskii, V. Semak, D. Opaitis, M. Shneider, R. Miles, and S. Macheret. The role of

- the photoionization in the numerical modeling of the dbd plasma actuator. In *47th AIAA Aerospace Sciences Meeting including The New Horizons Forum and Aerospace Exposition*, page 841, 2009.
- [29] A. V. Likhanskii, M. N. Shneider, S. O. Macheret, and R. B. Miles. Modeling of dielectric barrier discharge plasma actuator in air. *Journal of Applied Physics*, 103(5):053305, 2008.
- [30] J.-C. Matéo-Vélez. *Modélisation et simulation numérique de la génération de plasma dans les décharges couronnées et de son interaction avec l'aérodynamique*. PhD thesis, Toulouse, ENSAE, 2006.
- [31] F. R. Menter. Two-equation eddy-viscosity turbulence models for engineering applications. *AIAA journal*, 32(8):1598–1605, 1994.
- [32] A. Mesbah and D. B. Graves. Machine learning for modeling, diagnostics, and control of non-equilibrium plasmas. *Journal of Physics D: Applied Physics*, 52(30):30LT02, 2019.
- [33] E. Moreau. Airflow control by non-thermal plasma actuators. *Journal of Physics D: Applied Physics*, 40(3):605, 2007.
- [34] E. Moreau, P. Audier, and N. Benard. Ionic wind produced by positive and negative corona discharges in air. *Journal of Electrostatics*, 93:85–96, 2018.
- [35] E. Moreau, P. Audier, T. Orriere, and N. Benard. Electrohydrodynamic gas flow in a positive corona discharge. *Journal of Applied Physics*, 125(13):133303, 2019.
- [36] A. Mushyam, F. Rodrigues, and J. Pascoa. A plasma-fluid model for ehd flow in dbd actuators and experimental validation. *International Journal for Numerical Methods in Fluids*, 90(3):115–139, 2019.
- [37] K. Nakai, A. Nakano, and H. Nishida. Validity of three-fluid plasma modeling for alternating-current dielectric-barrier-discharge plasma actuator. *AIAA Journal*, pages 1–15, 2021.
- [38] K. Nakai and H. Nishida. Effects of numerical plasma modeling on performance characterization of plasma actuator. In *AIAA Scitech 2020 Forum*, page 1166, 2020.
- [39] M. Neumann, C. Friedrich, J. Czarske, J. Kriegseis, and S. Grundmann. Determination of the phase-resolved body force produced by a dielectric barrier discharge plasma actuator. *Journal of Physics D: Applied Physics*, 46(4):042001, 2012.
- [40] H. Nishida, T. Nonomura, and T. Abe. Three-dimensional simulations of discharge plasma evolution on a dielectric barrier discharge plasma actuator. *Journal of Applied Physics*, 115(13):133301, 2014.
- [41] D. M. Orlov. *Modelling and simulation of single dielectric barrier discharge plasma actuators*. 2006.
- [42] C. A. Pavan. *Reduced order modelling of streamers and their characterization by macroscopic parameters*. PhD thesis, Massachusetts Institute of Technology, 2019.
- [43] M. Sato, H. Aono, A. Yakeno, T. Nonomura, K. Fujii, K. Okada, and K. Asada. Multifactorial effects of operating conditions of dielectric-barrier-discharge plasma actuator on laminar-separated-flow control. *AIAA journal*, 53(9):2544–2559, 2015.
- [44] S. Sato, M. Takahashi, and N. Ohnishi. Enhanced electrohydrodynamic force generation in a two-stroke cycle dielectric-barrier-discharge plasma actuator. *Applied Physics Letters*, 110(19):194101, 2017.
- [45] U. Seth, P. Traoré, F. Duran-Olivencia, E. Moreau, and P. Vazquez. Parametric study of a dbd plasma actuation based on the suzen-huang model. *Journal of Electrostatics*, 93:1–9, 2018.
- [46] C. Shi, K. Adamiak, and G. Castle. Numerical study of the characteristics of a dielectric barrier discharge plasma actuator. *Journal of Physics D: Applied Physics*, 51(9):095201, 2018.
- [47] Y. Suzen, G. Huang, and D. Ashpis. Numerical simulations of flow separation control in low-pressure turbines using plasma actuators. In *45th AIAA Aerospace Sciences Meeting and Exhibit*, page 937, 2007.
- [48] Y. Suzen, G. Huang, J. Jacob, and D. Ashpis. Numerical simulations of plasma based flow control applications. In *35th AIAA Fluid Dynamics Conference and Exhibit*, page 4633, 2005.
- [49] H. G. Weller, G. Tabor, H. Jasak, and C. Fureby. A tensorial approach to computational continuum mechanics using object-oriented techniques. *Computers in physics*, 12(6):620–631, 1998.
- [50] H. Xu, N. Gomez-Vega, D. R. Agrawal, and S. R. Barrett. Higher thrust-to-power with large electrode gap spacing electroaerodynamic devices for aircraft propulsion. *Journal of Physics D: Applied Physics*, 53(2):025202, 2019.
- [51] H. Xu, Y. He, and S. R. Barrett. A dielectric barrier discharge ion source increases thrust and efficiency of electroaerodynamic propulsion. *Applied Physics Letters*, 114(25):254105, 2019.
- [52] H. Xu, Y. He, K. L. Strobel, C. K. Gilmore, S. P. Kelley, C. C. Hennick, T. Sebastian, M. R. Woolston, D. J. Perreault, and S. R. Barrett. Flight of an aeroplane with solid-state

- 1
2
3
4
5
6 propulsion. *Nature*, 563(7732):532–535, 2018.
7 [53] X. ZHANG, Y. CUI, C. M. J. TAY, and B. KHOO. Flow field generated by a dielectric barrier
8 discharge plasma actuator in quiescent air at initiation stage. *Chinese Journal of Aeronautics*,
9 2020.
10
11
12
13
14
15
16
17
18
19
20
21
22
23
24
25
26
27
28
29
30
31
32
33
34
35
36
37
38
39
40
41
42
43
44
45
46
47
48
49
50
51
52
53
54
55
56
57
58
59
60